Science in China Series G: Physics, Mechanics & Astronomy

www.scichina.com
phys.scichina.com
www.springerlink.com

Heavy-ion fusion and scattering with Skyrme energy density functional

WANG Ning[1†], LIU Min[1,2] & YANG YongXu[1]

[1] College of Physics and Technology, Guangxi Normal University, Guilin 541004, China;
[2] Institute of Low Energy Nuclear Physics, Beijing Normal University, Beijing 100875, China;

In our recent studies, an empirical barrier distribution was proposed for a unified description of the fusion cross sections of light and medium-heavy fusion systems, the capture cross sections of the reactions leading to superheavy nuclei, and the large-angle quasi-elastic scattering cross sections based on the Skyrme energy-density functional approach. In this paper, we first give a brief review of these results. Then, by examining the barrier distributions in detail, we find that the fusion cross sections depend more strongly on the shape of the left side of the barrier distribution while the quasi-elastic scattering cross sections depend more strongly on the right side. Furthermore, by combining these studies and the HIVAP calculations for the survival probability, the formation probability of the compound nucleus is deduced from the measured evaporation residue cross sections for "cold" and "hot" fusion reactions.

energy-density functional, fusion, fission, scattering, superheavy nuclei

In our recently published papers[1−5], we proposed an approach for a unified description of the fusion cross sections of light and medium-heavy fusion systems, the capture cross sections of the reactions leading to superheavy nuclei, and the large-angle quasi-elastic scattering cross sections based on the Skyrme energy-density functional approach. In this paper, we first give a brief review of this approach. Then, the influence of the shape of the barrier distribution on fusion cross sections and quasi-elastic scattering cross sections is studied carefully. Finally, we attempt to deduce the formation probability of compound nucleus from the measured evaporation residue cross sections of superheavy nuclei combining the proposed approach.

It is known that theoretical support for the time-consuming experiments to produce superheavy nuclei is vital in choosing the optimum target-projectile-energy combinations, and for the estimation of cross sections of evaporation residues. In the practical calculation of the evaporation residue cross section, the reaction process leading to the synthesis of superheavy nuclei is divided into two or three steps[6−9]. The simplified version of the

Received May 3, 2009; accepted May 22, 2009
doi: 10.1007/s11433-009-0205-z
†Corresponding author (email: wangning@gxnu.edu.cn)
Supported by the National Natural Science Foundation of China (Grant Nos. 10875031, 10847004, and 10865002) and the Alexander von Humboldt Foundation

Citation: Wang N, Liu M, Yang Y X. Heavy-ion fusion and scattering with Skyrme energy density functional. Sci China Ser G, 2009, 52(10): 1554-1573, doi: 10.1007/s11433-009-0205-z

evaporation residue cross section is given by

$$\sigma_{\rm ER}(E_{\rm c.m.}) = \sigma_{\rm cap}(E_{\rm c.m.})P_{\rm CN}(E_{\rm c.m.})W_{\rm sur}(E_{\rm c.m.}). \quad (1)$$

Here, $\sigma_{\rm cap}$, $P_{\rm CN}$ and $W_{\rm sur}$ are the capture cross section for the transition of the colliding nuclei over the entrance channel Coulomb barrier, the probability of the compound nucleus formation after the capture and the survival probability of the excited compound nucleus, respectively. There are several unsolved questions in each component of the right side of eq. (1) which leave a certain margin of uncertainty in the estimates of the evaporation residue cross section[10]. In addition, there could be several parameters in the practical models which are hardly unambiguously determined by a very limited number of measured evaporation residue cross sections of superheavy nuclei. For example, the calculated formation probability $P_{\rm CN}$ of the compound nuclei for reaction ^{58}Fe+^{208}Pb in ref. [7] is of about two orders of magnitude larger than that obtained in ref. [8], both of the models can, however, reproduce the measured evaporation residue cross sections satisfactorily. Therefore, it is very necessary to test and determine the interaction and parameters adopted in each component of eq. (1) individually.

To study the three components in eq. (1) individually, we first investigate the influence of the fission and quasi-fission on the fusion-fission reactions. It is generally thought that for systems with the compound-nuclear charge number $Z_{\rm CN}$ smaller than about 60, the fission barrier is high enough to make fission an improbable decay mode at incident energies close to the fusion barrier[11]. Thus for these reactions, $\sigma_{\rm ER} \simeq \sigma_{\rm fus} \simeq \sigma_{\rm cap}$ holds at near-barrier energies. To see it more clearly, we present a schematic figure (Figure 1). The horizontal and vertical axes denote the compound-nuclear charge number $Z_{\rm CN}$ and the mass asymmetry of the reaction system $\eta = (A_2 - A_1)/(A_2 + A_1)$, respectively. Here, A_1 and A_2 are the projectile and target masses. The fusion reactions in region I have $P_{\rm CN} \simeq W_{\rm sur} \simeq 1$ as discussed before. There are quite a large number of experimental data of evaporation residue cross sections for the reactions in region I accumulated in recent decades, which makes it possible to establish a reliable model for systematic description of the capture process without the influence of fission and quasi-fission. For heavier compound systems the fission increases rapidly with the $Z_{\rm CN}^2/A_{\rm CN}$ and the angular momentum. For sufficiently asymmetric systems with $Z_{\rm CN}$ well below 100 (systems in region II of Figure 1), and at energies close to the fusion barrier, it is generally recognized that $\sigma_{\rm fus} = \sigma_{\rm ER} + \sigma_{\rm FF}$. Here the $\sigma_{\rm fus}$, $\sigma_{\rm ER}$ and $\sigma_{\rm FF}$ are the cross sections for fusion, evaporation residue and fission, respectively. For systems in region II, it is thought that the quasi-fission barrier is high enough and thus $P_{\rm CN} \simeq 1$. The available experimental data of the evaporation residue cross sections for reactions in region II are less than those in region I, but they seem to be much enough for a systematic investigation to test and determine some key parameters of a statistical model for calculating the survival probability $W_{\rm sur}$, combining the model for describing the capture cross sections, without the influence of the quasi-fission. In addition, the measured fusion cross sections for reactions in region II can further test the theoretical model for calculating $\sigma_{\rm cap}$. For $Z_{\rm CN}$ larger than about 100 (systems in region III of Figure 1), quasi-fission occurs. Thus in the calculation of the evaporation residue cross sections for these reactions, the influence of quasi-fission should be taken into account ($P_{\rm CN} < 1$). If both $\sigma_{\rm cap}$ and $W_{\rm sur}$ can be predicted reliably, the fusion (formation) probability $P_{\rm CN}$ of compound

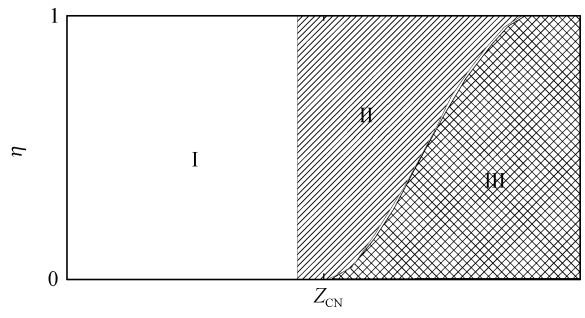

Figure 1 A schematic figure for different types of fusion reactions. The horizontal and vertical axes denote the compound-nuclear charge number $Z_{\rm CN}$ and the mass asymmetry of the reaction system $\eta = (A_2 - A_1)/(A_2 + A_1)$, respectively.

nucleus could be deduced from the measured evaporation residue cross sections of superheavy nuclei which is important to check and develop theoretical model for describing $P_{\rm CN}$, and to understand the dynamics of fusion and quasi-fission.

In addition, it is found that both the heavy-ion fusion and quasi-elastic scattering at energies around the Coulomb barrier can provide an ideal opportunity to obtain the information of nucleus-nucleus interaction which plays a key role to the mechanism of fusion reactions and is of great importance for the synthesis of super-heavy nuclei. Based on the quantum tunnelling concept, it is thought that the quasi-elastic scattering (a sum of elastic, inelastic scattering, and transfer channels) is a good counterpart of the fusion reaction in the sense that the former is related to the reflection probability of a potential barrier while the latter is related to the penetration probability[12]. In addition, it has been shown that the fusion barrier distribution generated by the coupling of the relative motion of the nuclei to internal degrees of freedom can be extracted from precisely measured fusion excitation functions[13,14]. The similarity of the barrier distribution can be extracted from large-angle quasi-elastic scattering excitation functions[15] which can be more easily measured than the fusion excitation functions[16]. Therefore, it is also necessary to investigate the nucleus-nucleus potential and the barrier distribution through the heavy-ion large-angle quasi-elastic scattering.

Based on the above discussions, the main aim of this work is to establish a theoretical model to calculate the fusion (capture) cross sections of heavy-ion fusion reactions, which is the first and essential step to study the mechanism of synthesis of superheavy nuclei. In this model, the Skyrme energy density functional is applied to make a systematic study of fusion reactions. Firstly, we will use the semi-classical expressions of the Skyrme energy density functional to study the energies and the density distributions of a series of nuclei by the restricted density variational (RDV) method[17−19]. Secondly, with the density distributions obtained, the entrance-channel potentials of a series of fusion reactions are calculated. Then, based on the entrance-channel potential obtained, an empirical barrier distribution is proposed to take into account the multi-dimensional character of real barrier, and then apply it to calculate the fusion excitation functions in terms of barrier penetration concept. In addition, the empirical barrier distribution is further tested for describing the large-angle quasi-elastic scattering reactions. Furthermore, this approach is extended to study the fusion-fission reactions in which the quasi-fission is not important. To study this kind of reactions we employ the Skyrme energy density functional approach to obtain the capture cross sections of the reactions. For calculation of $W_{\rm sur}$, the well-known standard statistical model (with HIVAP code[11,20,21]) is used. The evaporation residue cross sections of a series of fusion-fission reactions will be investigated for a systematic test of the model and refining the parameters. Finally, the formation probability of compound nucleus will be deduced from the measured evaporation cross sections.

1 The model for description of fusion cross section

The energy density functional theory is widely used in many-body problems. In the framework of the semi-classical Extended Thomas Fermi (ETF) approach together with a Skyrme effective nuclear interaction, the energy density functional can be derived systematically. We take the Skyrme Hartree-Fock (Skyrme HF) formalism of the energy density functional[18,22] and based on it we calculate the proton and neutron densities of nuclei by means of restricted density variational method[17−19]. With the neutron and proton densities determined in this way we calculate the fusion barrier for fusion reaction based on the same energy density functional. Then, based on the fusion barrier obtained, an empirical barrier distribution is proposed to calculate the fusion excitation functions in terms of barrier penetration concept.

1.1 Skyrme energy density functional

The total binding energy of a nucleus can be expressed as the integral of energy density

functional[19,22]

$$E = \int \mathcal{H}\, \mathrm{d}\boldsymbol{r}. \tag{2}$$

The energy density functional $\mathcal{H}$ includes the kinetic, nuclear interaction and Coulomb interaction energy parts

$$\mathcal{H} = \frac{\hbar^2}{2m}[\tau_{\mathrm{p}}(\boldsymbol{r}) + \tau_{\mathrm{n}}(\boldsymbol{r})] + \mathcal{H}_{\mathrm{sky}}(\boldsymbol{r}) + \mathcal{H}_{\mathrm{coul}}(\boldsymbol{r}). \tag{3}$$

For the kinetic energy part, the extended Thomas-Fermi (ETF) approach includes all terms up to the second order in the spatial derivatives (ETF2). With the effective-mass form factor

$$\begin{aligned} f_i(\boldsymbol{r}) &= 1 + \frac{2m}{\hbar^2}\left\{\frac{1}{4}\left[t_1\left(1+\frac{x_1}{2}\right) + t_2\left(1+\frac{x_2}{2}\right)\right]\rho(\boldsymbol{r}) \right. \\ &\left. + \frac{1}{4}\left[t_2\left(x_2+\frac{1}{2}\right) - t_1\left(x_1+\frac{1}{2}\right)\right]\rho_i(\boldsymbol{r})\right\}, \end{aligned} \tag{4}$$

the kinetic energy densities τ for protons ($i = p$) and neutrons ($i = n$) are given by

$$\begin{aligned} \tau_i(\boldsymbol{r}) = {} & \frac{3}{5}(3\pi^2)^{2/3}\rho_i^{5/3} + \frac{1}{36}\frac{(\nabla\rho_i)^2}{\rho_i} + \frac{1}{3}\Delta\rho_i \\ & + \frac{1}{6}\frac{\nabla\rho_i\nabla f_i + \rho_i\Delta f_i}{f_i} - \frac{1}{12}\rho_i\left(\frac{\nabla f_i}{f_i}\right)^2 \\ & + \frac{1}{2}\rho_i\left(\frac{2m}{\hbar^2}\frac{W_0}{2}\frac{\nabla(\rho+\rho_i)}{f_i}\right)^2, \end{aligned} \tag{5}$$

where ρ_i denotes the proton or neutron density of the nucleus and $\rho = \rho_{\mathrm{p}} + \rho_{\mathrm{n}}$, $\tau = \tau_{\mathrm{p}} + \tau_{\mathrm{n}}$, W_0 denotes the strength of the Skyrme spin-orbit interaction. The nuclear interaction part with Skyrme interaction $\mathcal{H}_{\mathrm{sky}}$ reads

$$\begin{aligned} &\mathcal{H}_{\mathrm{sky}}(\boldsymbol{r}) \\ &= \frac{t_0}{2}\left[\left(1+\frac{1}{2}x_0\right)\rho^2 - \left(x_0+\frac{1}{2}\right)(\rho_{\mathrm{p}}^2+\rho_{\mathrm{n}}^2)\right] \\ &+ \frac{1}{12}t_3\rho^\alpha\left[\left(1+\frac{1}{2}x_3\right)\rho^2 - \left(x_3+\frac{1}{2}\right)(\rho_{\mathrm{p}}^2+\rho_{\mathrm{n}}^2)\right] \\ &+ \frac{1}{4}\left[t_1\left(1+\frac{1}{2}x_1\right) + t_2\left(1+\frac{1}{2}x_2\right)\right]\tau\rho \\ &+ \frac{1}{4}\left[t_2\left(x_2+\frac{1}{2}\right) - t_1\left(x_1+\frac{1}{2}\right)\right](\tau_{\mathrm{p}}\rho_{\mathrm{p}} + \tau_{\mathrm{n}}\rho_{\mathrm{n}}) \\ &+ \frac{1}{16}\left[3t_1\left(1+\frac{1}{2}x_1\right) - t_2\left(1+\frac{1}{2}x_2\right)\right](\nabla\rho)^2 \\ &- \frac{1}{16}\left[3t_1\left(x_1+\frac{1}{2}\right) + t_2\left(x_2+\frac{1}{2}\right)\right] \\ &\times [(\nabla\rho_{\mathrm{n}})^2 + (\nabla\rho_{\mathrm{p}})^2] - \frac{W_0^2}{4}\frac{2m}{\hbar^2} \\ &\times \left[\frac{\rho_{\mathrm{p}}}{f_{\mathrm{p}}}(2\nabla\rho_{\mathrm{p}} + \nabla\rho_{\mathrm{n}})^2 + \frac{\rho_n}{f_{\mathrm{n}}}(2\nabla\rho_{\mathrm{n}} + \nabla\rho_{\mathrm{p}})^2\right], \end{aligned} \tag{6}$$

where t_0, t_1, t_2, t_3, x_0, x_1, x_2, x_3,and α are Skyrme-force parameters. The last term in the right hand of expression (6) is the semi-classical expansions (up to second order in $\hbar$) of spin-orbit densities[22]. The Coulomb energy density can be written as the sum of the direct and exchange contribution, the latter being taken into account in the Slater approximation,

$$\begin{aligned} \mathcal{H}_{\mathrm{Coul}}(\boldsymbol{r}) = {} & \frac{e^2}{2}\rho_{\mathrm{p}}(\boldsymbol{r})\int \frac{\rho_{\mathrm{p}}(\boldsymbol{r}')}{|\boldsymbol{r}-\boldsymbol{r}'|}\mathrm{d}\boldsymbol{r}' \\ & - \frac{3e^2}{4}\left(\frac{3}{\pi}\right)^{1/3}(\rho_{\mathrm{p}}(\boldsymbol{r}))^{4/3}. \end{aligned} \tag{7}$$

From the above expressions (2)–(7), one can see that the total energy of a nuclear system can be expressed as a functional of protons and neutrons densities [$\rho_{\mathrm{p}}(\boldsymbol{r})$, $\rho_{\mathrm{n}}(\boldsymbol{r})$] under the Skyrme interaction associated with the ETF approximation.

1.2 Neutron and proton densities of nuclei

By minimizing the total energy of the system given by expression (2), the neutron and proton densities can be obtained, that is to solve the variational equation:

$$\begin{aligned} &\frac{\delta}{\delta\rho_i}\int\{\mathcal{H}[\rho_{\mathrm{n}}(\boldsymbol{r}),\rho_{\mathrm{p}}(\boldsymbol{r})] - \lambda_{\mathrm{n}}\rho_{\mathrm{n}}(\boldsymbol{r}) - \lambda_{\mathrm{p}}\rho_{\mathrm{p}}(\boldsymbol{r})\}\,\mathrm{d}\boldsymbol{r} \\ &= 0, \end{aligned} \tag{8}$$

with the Lagrange multipliers λ_{n} and λ_{p} to ensure the conservation of neutron and proton number. This density variational problem has been solved in two different ways in the past: either by resolving the Euler-Lagrange equation[17] resulting from eq. (8) or by carrying out the variational calculation in a restricted subspace of functions[17–19]. In this work we take the neutron and proton density distributions of a nucleus as spherical symmetric Fermi functions

$$\rho_i(\boldsymbol{r}) = \rho_{0i}\left[1 + \exp\left(\frac{r-R_i}{a_i}\right)\right]^{-1}, \quad i = \{n,p\}. \tag{9}$$

For the three quantities ρ_{0i}, R_i and a_i in the equation, only two of them are independent because of the conservation of particle number $N_i =$

$\int \rho_i(\boldsymbol{r})\mathrm{d}(\boldsymbol{r})$, $N_i = \{N, Z\}$. In other words,

$$\rho_{0i} = N_i \left[\int \frac{\mathrm{d}\boldsymbol{r}}{1 + \exp\left(r - R_i\right)/a_i} \right]^{-1}. \qquad (10)$$

Here, R_p, a_p R_n, a_n are the radius and diffuseness for proton and neutron density distributions, respectively. By using optimization algorithm, one can obtain the minimal energy E as well as the corresponding R_p, a_p, R_n, a_n for the neutron and proton density distributions.

The Skyrme force SkM*[24] is adopted in the calculations since SkM* is very successful for describing the bulk properties and surface properties of nuclei. In Figure 2 we show the relative deviations of the calculated charge root-mean-square radii for a series of nuclei from the experimental data. The obtained charge root-mean-square radii in this work for shell closed nuclei are very close to the corresponding experimental data. We also find that the neutron skin thickness of nuclei can be described well with this approach[25].

1.3 Calculations of fusion barriers

The interaction potential $V(R)$ between reaction partners can be written as

$$V(R) = E_\mathrm{tot}(R) - E_1 - E_2, \qquad (11)$$

where R is the center-to-center distance between two nuclei, the $E_\mathrm{tot}(R)$ is the total energy of the interacting nuclear system, E_1 and E_2 are the energies of individual nuclei (projectile and target at an infinite distance), respectively. The interaction potential $V(R)$ is also called entrance-channel potential in ref. [23] or fusion barrier, in the following we take the term of fusion barrier. The $E_\mathrm{tot}(R)$, E_1, E_2 are calculated with the same energy-density functional as that is used in the calculations of nuclear densities,

$$E_\mathrm{tot}(R) = \int \mathcal{H}[\rho_{1\mathrm{p}}(\boldsymbol{r}) + \rho_{2\mathrm{p}}(\boldsymbol{r} - \boldsymbol{R}), \rho_{1\mathrm{n}}(\boldsymbol{r}) + \rho_{2\mathrm{n}}(\boldsymbol{r} - \boldsymbol{R})]\ \mathrm{d}\boldsymbol{r},$$

$$E_1 = \int \mathcal{H}[\rho_{1\mathrm{p}}(\boldsymbol{r}), \rho_{1\mathrm{n}}(\boldsymbol{r})]\mathrm{d}\boldsymbol{r}, \qquad (12)$$

$$E_2 = \int \mathcal{H}[\rho_{2\mathrm{p}}(\boldsymbol{r}), \rho_{2\mathrm{n}}(\boldsymbol{r})]\ \mathrm{d}\boldsymbol{r}. \qquad (13)$$

Here, ρ_{1p}, ρ_{2p}, ρ_{1n} and ρ_{2n} are the frozen proton and neutron densities of the projectile and target, determined in the previous section.

For a certain reaction system, the entrance-channel potential is calculated in a range from $R = 7$ fm to 15 fm with a step size ΔR =0.25 fm. Figure 3 shows the entrance-channel potential of ^{48}Ca+^{208}Pb, ^{128}Sb+^{128}Sb and ^{16}O+^{240}Pu. The solid, crossed and dashed curves denote the results of this approach and of the proximity potential[26] and modified Woods-Saxon potential (see sec. 2), respectively. The results of Skyrme energy-density functional approach are generally close to those of proximity potential in the region where the densities of the two nuclei do not overlap. The barrier height B_0, radius R_0 and the curvature $\hbar\omega_0$ near R_0 as well as the position of fusion pocket R_s can be obtained from the calculations (see Figure 3). Here, the curvature $\hbar\omega_0$ of the barrier is obtained through fitting the entrance-channel potential in the region from $R_0 - 1.25$ fm to $R_0 + 1.25$ fm by an inverted parabola (if $R_0 - 1.25$ fm$< R_\mathrm{s}$, then from R_s to $R_0 + 1.25$ fm). We would like to emphasize that the fusion barrier is obtained without any adjustable parameters in this approach.

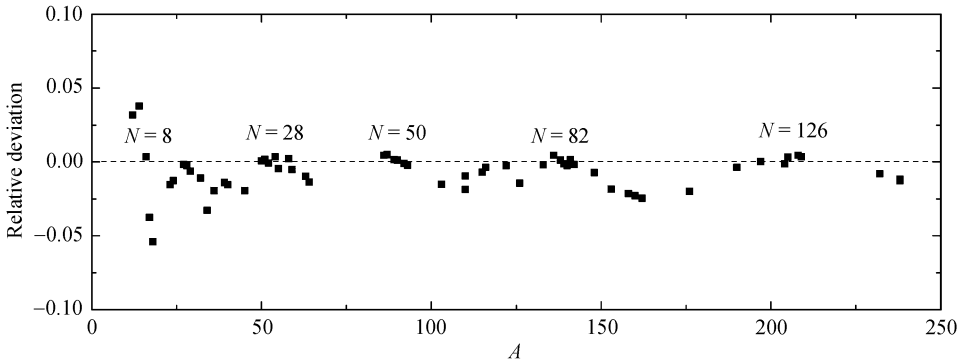

Figure 2 Relative deviations of the calculated charge root-mean-square radii for a series of nuclei from the experimental data.

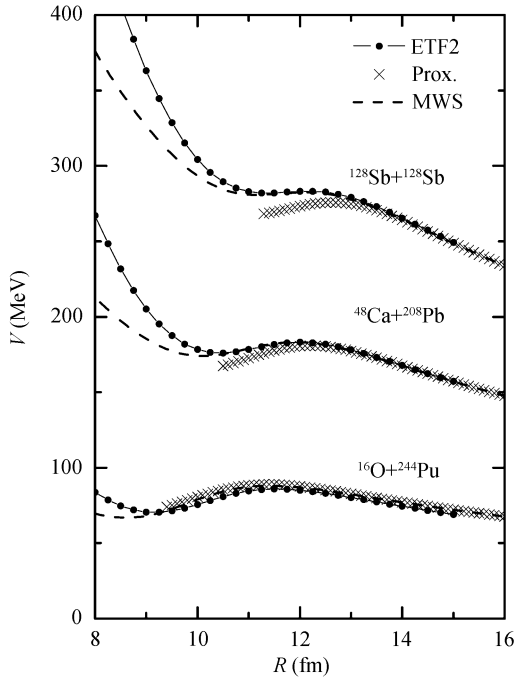

Figure 3 The entrance-channel potential for reactions ^{48}Ca+^{208}Pb, ^{128}Sb+^{128}Sb and ^{16}O+^{240}Pu. The solid and dashed curves denote the results of Skyrme energy density functional within ETF2 and modified Woods-Saxon potential. The crossed curves denote the proximity potential. The compound nucleus of the three system is ^{256}No.

1.4 Empirical barrier distribution

For fusion reactions with heavy-ions, it is known that the coupling of other degrees of freedom (such as deformation and vibration of nuclei) to the distance between two nuclei is obvious. We take into account the multi-dimensional character of realistic barrier due to the coupling to internal degrees of freedom of the binary system empirically. We assume that the one-dimensional barrier is replaced by a distribution of fusion barrier $D(B)$. The distribution function $D(B)$ satisfies

$$\int_0^\infty D(B)\mathrm{d}B = 1. \tag{14}$$

Motivated by the shape of the barrier distribution extracted from experiments, we consider the weight function to be a superposition of two Gaussian functions $D_1(B)$ and $D_2(B)$, which read

$$D_1(B) = \frac{1}{2\sqrt{g\pi}w_1}\exp\left[-\frac{(B-B_1)^2}{g\,(2w_1)^2}\right], \tag{15}$$

and

$$D_2(B) = \frac{1}{2\sqrt{\pi}w_2}\exp\left[-\frac{(B-B_2)^2}{(2w_2)^2}\right], \tag{16}$$

with

$$B_1 = B_\mathrm{c} + w_1, \tag{17}$$

$$B_2 = B_\mathrm{c} + w_2, \tag{18}$$

$$w_1 = \frac{1}{4}(B_0 - B_\mathrm{c}), \tag{19}$$

$$w_2 = \frac{1}{2}(B_0 - B_\mathrm{c}). \tag{20}$$

Here B_0 is the barrier height from the entrance channel potential obtained above. We set $B_\mathrm{c} = 0.926B_0$. From the expressions of (15) and (16) one can find that the peaks and the widths of $D_1(B)$ and $D_2(B)$ only depend on the height of the fusion barrier B_0 except the g in $D_1(B)$. The quantity g in $D_1(B)$ is a factor which empirically takes into account the structure effects and has a value $0 < g \leqslant 2$. The larger the value of g is, the larger the fusion cross section at sub-barrier energies is. For the fusion reactions with neutron-shell open nuclei but near the β-stability line we set $g = 1$. From a systematic investigation we learn that for the reactions with neutron-shell closed nuclei we have $0 < g < 1$ while for the reactions with neutron-rich nuclei $1 < g \leqslant 2$. The enhancement of fusion cross sections for reactions with neutron-rich nuclei ($1 < g \leqslant 2$) compared with non-neutron-rich nuclei has been found in refs. [27–29]. It is attributed to the neutron transfer and neck formation which lower the fusion barrier and thus enhance the fusion cross sections at sub-barrier energies[27,29]. For neutron closed-shell nuclei ($0 < g < 1$), the strong shell effect suppresses the lowering barrier effect. For the reactions with neutron-shell closed nuclei or neutron-rich nuclei an empirical formula for the g values is proposed,

$$g = \left[1 - c_0\Delta Q + 0.5(\delta_n^{\mathrm{prog}} + \delta_n^{\mathrm{targ}})\right]^{-1}, \tag{21}$$

where $\Delta Q = Q - Q_0$ denotes the difference between the Q-value of the system under consideration for complete fusion and that of the reference system. The Q_0 is the Q-value of reference system. $c_0 = 0.5$ MeV^{-1} for $\Delta Q < 0$ cases and $c_0 = 0.1$ MeV^{-1} for $\Delta Q > 0$ cases. $\delta_n^{\mathrm{proj(targ)}} = 1$ for neutron closed-shell projectile (target) nucleus and $\delta_n^{\mathrm{proj(targ)}} = 0$

for non-closed cases (the shell-closure effects of ^{16}O are neglected in this work). In addition, we introduce a truncation for g value, i.e. g should not be larger than 2. The reference system is chosen to be the reaction system with nuclei along the β-stability line. More detailed introduction is in ref. [1].

With the $D_1(B)$ and $D_2(B)$, an effective weight function $D_{\rm eff}(B)$, by which the fusion excitation function can be calculated, is proposed,

$$D_{\rm eff}(B) = \begin{cases} D_1(B): & B < B_x, \\ D_{\rm avr}(B): & B \geqslant B_x, \end{cases} \quad (22)$$

with $D_{\rm avr}(B) = (D_1(B) + D_2(B))/2$. The B_x denotes the position of the left crossing point between $D_1(B)$ and $D_{\rm avr}(B)$.

It was shown in refs. [13,13,28] that the distribution of the fusion barrier heights could be extracted directly from a fusion excitation function using the second derivative of the product of cross section $\sigma_{\rm fus}$ multiplied by the energy E, i.e.

$$D_{\rm fus}(E) = \frac{1}{\pi R_{\rm fus}^2} \frac{{\rm d}^2(E\sigma_{\rm fus})}{{\rm d}E^2}. \quad (23)$$

The differentiation is performed using the point-difference approximation[14,28]. In Figure 4 we present a comparison between the extracted fusion barrier distributions $D_{\rm fus}$ and the empirical ones $D_{\rm eff}$ for the reactions ^{12}C+^{92}Zr, ^{19}F+^{208}Pb and ^{16}O+^{144,154}Sm[3]. The squares and the crossed curves denote the results for $D_{\rm fus}$ and $D_{\rm eff}$, respectively. The shapes of the fusion barrier distributions extracted from experimental data are well reproduced by the parametrization of the empirical barrier distribution proposed.

1.5 Calculations of fusion cross sections

With the proposed empirical barrier distribution, and the fusion radius $R_{\rm fus}$ and the curvature of the barrier $\hbar\omega$ obtained with the entrance channel fusion barrier, the fusion excitation function (or the capture excitation function of reactions in region III of Figure 1) can be obtained (details in ref. [1])

$$\sigma_{\rm fus}(E_{\rm c.m.}) = \min[\sigma_1(E_{\rm c.m.}), \sigma_{\rm avr}(E_{\rm c.m.})], \quad (24)$$

with

$$\sigma_1(E_{\rm c.m.}) = \int_0^\infty D_1(B)\, \sigma_{\rm fus}^{\rm Wong}(E_{\rm c.m.}, B){\rm d}B, \quad (25)$$

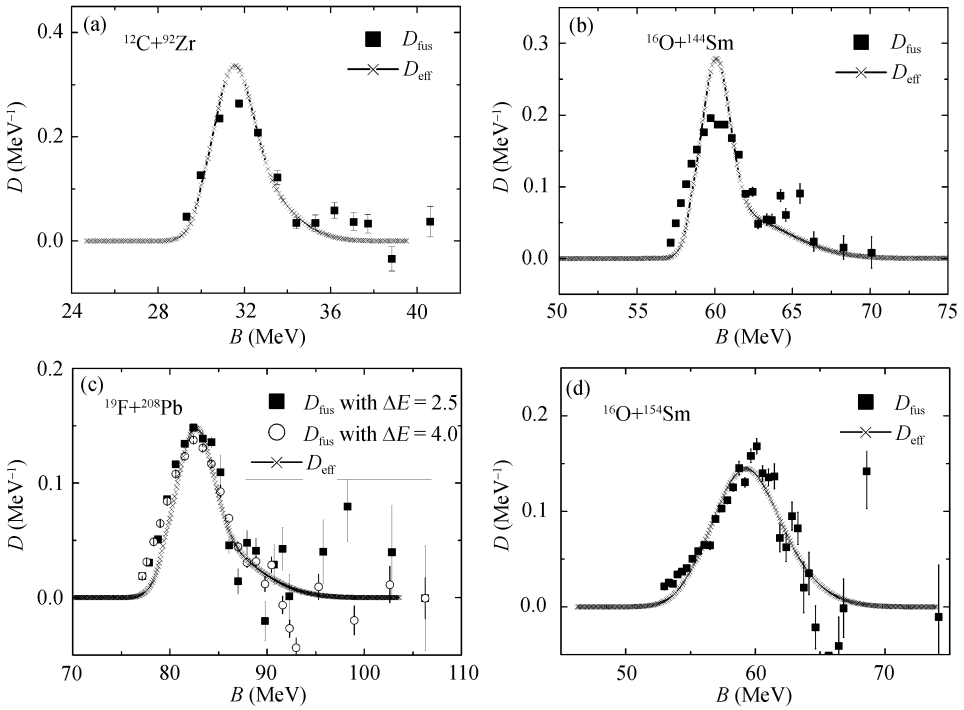

Figure 4 Fusion barrier distributions for the reactions ^{12}C+^{92}Zr, ^{19}F+^{208}Pb and ^{16}O+^{144,154}Sm. The squares and the crossed curves denote the results for $D_{\rm fus}$ and $D_{\rm eff}$, respectively.

and

$$\sigma_{\rm avr}(E_{\rm c.m.}) = \int_0^\infty \left[\frac{D_1(B)+D_2(B)}{2}\right] \sigma_{\rm fus}^{\rm Wong} \times (E_{\rm c.m.}, B){\rm d}B. \quad (26)$$

Here, $\sigma_{\rm fus}^{\rm Wong}$ denotes Wong's formula[30] for penetrating an one-dimensional parabolic barrier,

$$\sigma_{\rm fus}^{\rm Wong}(E_{\rm c.m.}, B_0) = \frac{\hbar\omega R_{\rm fus}^2}{2E_{\rm c.m.}} \ln\left(1+\exp\left[\frac{2\pi}{\hbar\omega}(E_{\rm c.m.}-B_0)\right]\right) \quad (27)$$

with the center-of-mass energy $E_{\rm c.m.}$. B_0, $R_{\rm fus}$ and $\hbar\omega$ are the barrier height, radius and curvature, respectively. The influence of angular momentum in the entrance channel has already been taken into account in Wong's formula with the assumption that the barrier position $R_{\rm fus}$ and the barrier curvature $\hbar\omega$ do not change with angular momentum.

Figure 5 shows some calculation results and experimental data for comparison for a series of fusion reactions[1]. More calculation results are given in refs. [1,2]. All the fusion excitation functions can be reproduced very well, which indicates our parametrization of $D_1(B)$ and $D_2(B)$ is quite useful and reasonable.

Further, we find that at energies near and above the fusion barrier, calculated fusion cross sections are not sensitive to the value of g which implies that we can calculate the fusion cross sections at energies near and above the fusion barrier for unmeasured fusion system by simply taking $g=1$ in the empirical barrier distribution. For sub-barrier fusion, more sophisticated investigation for g value is required. We have systematically calculated the fusion (capture) excitation functions of 120 fusion reactions at energies near and above the barrier (with $g=1$) and their average deviation $\chi^2_{\log}$ from the experimental data is defined as

$$\chi^2_{\log} = \frac{1}{m}\sum_{n=1}^{m}[\log(\sigma_{\rm th}(E_n)) - \log(\sigma_{\rm exp}(E_n))]^2. \quad (28)$$

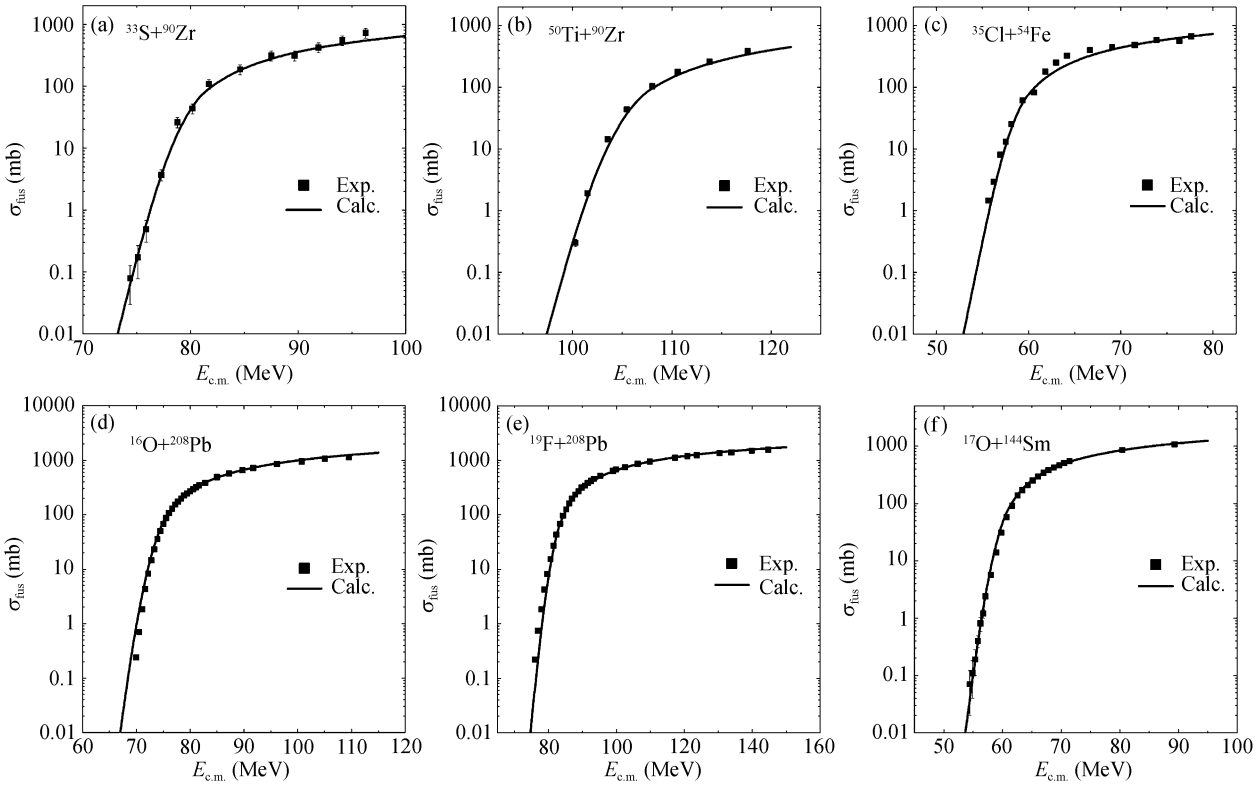

Figure 5 The fusion excitation functions for reactions ^{33}S,^{50}Ti+^{90}Zr, ^{35}Cl+^{54}Fe, ^{16}O,^{19}F+^{208}Pb and ^{17}O+^{144}Sm with neutron-shell closed nuclei near the β-stability line. The squares denote the experimental data. The solid denote the calculation results with the g values obtained by formula (21).

Here m denotes the number of energy-points of experimental data, and $\sigma_{\rm th}(E_n)$ and $\sigma_{\rm exp}(E_n)$ are the calculated and experimental fusion (capture) cross sections at the center-of-mass energy E_n ($E_n \geqslant B_0$), respectively. The calculated results[4] for $\chi^2_{\log}$ are shown in Figure 6. The average deviations of about 70% systems in $\chi^2_{\log}$ are less than 0.005, with which we can estimate the systematic error (about 18% of $\sigma_{\rm fus}$) of this approach for the description of the fusion (capture) cross sections at energies near and above the barriers. With $g \simeq 0$ and $g = 2$ we estimate the lower and upper limits of the fusion (capture) cross sections at sub-barrier energies respectively. From the calculation results, we can see that the empirical barrier distribution approach for description of fusion cross sections is simple, reliable and powerful. It provides a solid base for the study of unmeasured fusion reactions.

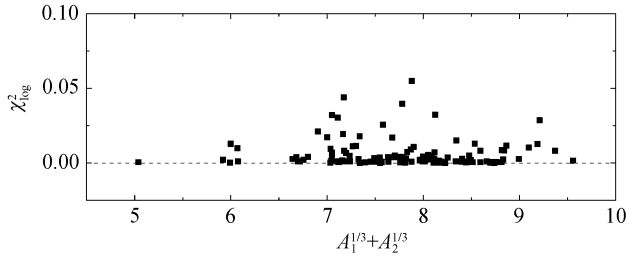

Figure 6 The average deviations $\chi^2_{\log}$ for a total of 120 fusion reactions. A_1 and A_2 denote the projectile and target masses, respectively.

2 Application of the model to quasi-elastic scattering reactions

In this section, we first introduce an empirical nucleus-nucleus potential based on the Skyrme energy density functional within the extended Thomas-Fermi approach. Then, the quasi-elastic scattering and the transfer probabilities are described with the empirical barrier distribution. Some calculated results are also presented in this section. Finally, we study the influence of the shape of the barrier distribution on fusion and quasi-elastic scattering.

2.1 Modified woods-saxon potential

The nucleus-nucleus interaction potential reads as

$$V(R) = V_{\rm N}(R) + V_{\rm C}(R). \qquad (29)$$

Here, $V_{\rm N}$ and $V_{\rm C}$ are the nuclear and Coulomb interactions, respectively. We take $V_{\rm C}(R) = e^2 Z_1 Z_2/R$, and the nuclear interaction $V_{\rm N}$ to be of Woods-Saxon form with five parameters determined by fitting the entrance channel potentials obtained in sec. 1.3.

$$V_N(R) = \frac{V_0}{1+\exp[(R-R_0)/a]}, \qquad (30)$$

with

$$V_0 = u_0[1+\kappa(I_1+I_2)]\frac{A_1^{1/3}A_2^{1/3}}{A_1^{1/3}+A_2^{1/3}}, \qquad (31)$$

and

$$R_0 = r_0(A_1^{1/3}+A_2^{1/3}) + c. \qquad (32)$$

$I_1 = (N_1 - Z_1)/A_1$ and $I_2 = (N_2 - Z_2)/A_2$ in eq. (31) are the isospin asymmetries of projectile and target nuclei, respectively.

By varying the five free parameters u_0, κ, r_0, c and a of the modified Woods-Saxon (MWS) potential, we minimize the relative deviation between the fusion barrier height obtained with the Skyrme energy-density functional with SkM*[24] force and the barrier height of the MWS potential obtained with eq. (29). The corresponding optimal values of these parameters are obtained at the minimum of the relative deviation. In this work, 66996 reactions with $Z_1 Z_2 \leqslant 3000$ were used to determine the parameters of the modified Woods-Saxon potential. The obtained optimal values of the parameters are listed in Table 1. Part of results with the MWS potential are shown in Figure 3 by the dashed curves.

Table 1 Parameters of the potential

r_0 (fm)	c (fm)	u_0 (MeV)	κ	a (fm)
1.27	−1.37	−44.16	−0.40	0.75

2.2 Elastic scattering at the above barrier energies

The proposed nucleus-nucleus potential is based on the frozen density approximation. The time-dependent Hartree-Forck (TDHF) calculations show that the nucleus-nucleus potential depends on the incident energy at energies close to the Coulomb barrier and when the center-of-mass energy is much higher than the Coulomb

barrier energy, potentials deduced with the microscopic theory identify with the frozen density approximation[31]. We test the modified Woods-Saxon potential for the description of heavy-ion elastic scattering at energies much higher than the Coulomb barrier, since the reaction time is relatively short and the frozen density approximation seems to be applicable at these energies. Based on the optical model, we solve the Schroedinger equation for a given nucleus-nucleus potential using the traditional Numerov method to obtain the partial-wave scattering matrix that is used to describe the elastic scattering data[32]. The real and imaginary parts of the optical potential adopted in the calculations are described by the modified Woods-Saxon potential.

We have calculated the elastic scattering angular distributions for the reactions ^{12}C+^{208}Pb, ^{16}O+^{208}Pb, ^{12}C+^{90}Zr and ^{16}O+^{63}Cu at different laboratory energies[5]. The calculated results (solid curves) are shown in Figure 7, and the corresponding experimental data (squares) are also presented for comparison. The experimental data of the four reactions at different energies are reasonably well reproduced by the modified Woods-Saxon potential in which the potential parameters are fixed.

2.3 Description of large-angle quasi-elastic scattering

As a good counterpart of the fusion reaction, the large-angle quasi-elastic scattering is studied to explore the nucleus-nucleus potential. In this work, we explore the influence of the empirical barrier distribution proposed for the fusion reactions on the large-angle quasi-elastic scattering.

It is thought that the quasi-elastic differential cross section can be expressed as a weighted sum of the eigenchannel elastic differential cross sections under the adiabatic and iso-centrifugal approximation[38,39]. Similarly to the description of fusion with the empirical barrier distribution, we describe the large-angle quasi-elastic scatter-

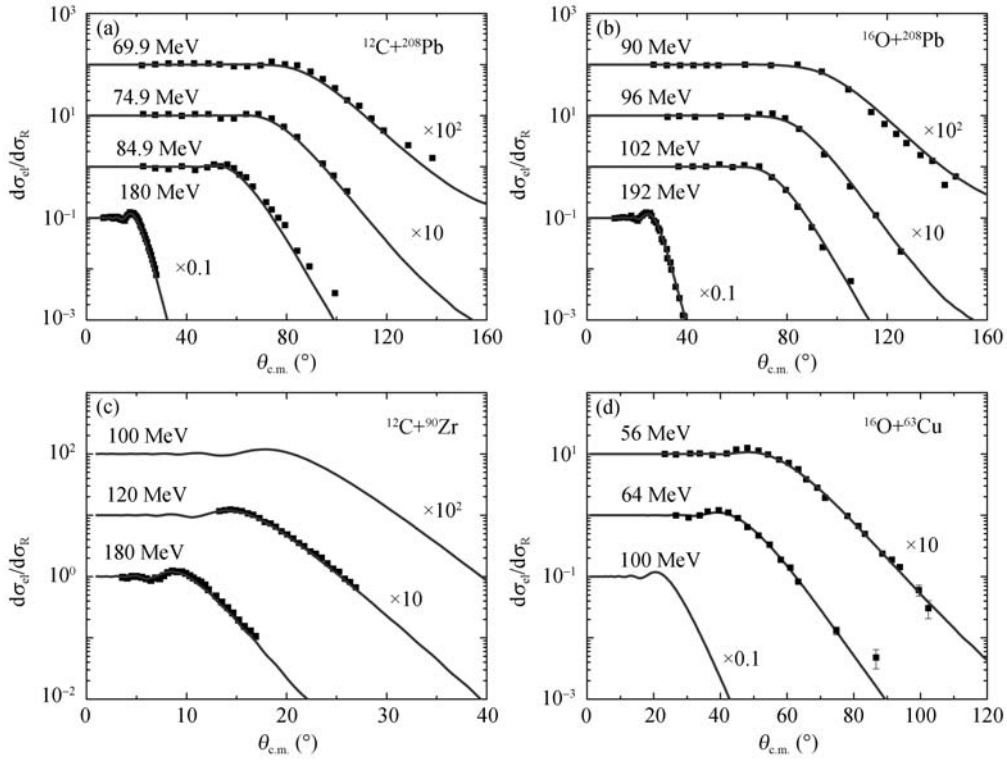

Figure 7 Elastic scattering angular distributions for the reactions ^{12}C+^{208}Pb, ^{16}O+^{208}Pb, ^{12}C+^{90}Zr and ^{16}O+^{63}Cu at different laboratory energies. The solid curves and the squares denote the calculated results with the modified Woods-Saxon potential and the experimental data, respectively. The experimental data are taken from refs. [33–37].

ing cross section with the effective weight function $D_{\rm eff}(B)$ at energies around the Coulomb barrier:

$$\frac{{\rm d}\sigma_{\rm qel}}{{\rm d}\sigma_{\rm R}}(E_{\rm c.m.}) = P_{\rm eff} + P_{\rm corr}, \quad (33)$$

with

$$P_{\rm eff} = \frac{1}{F_0}\int_0^\infty D_{\rm eff}(B)\frac{{\rm d}\sigma_{\rm el}}{{\rm d}\sigma_{\rm R}}(E_{\rm c.m.}, B){\rm d}B, \quad (34)$$

and $P_{\rm corr}$ is a small correction term. ${\rm d}\sigma_{\rm el}/{\rm d}\sigma_R$ is the ratio of the elastic cross section $\sigma_{\rm el}$ to the Rutherford cross section $\sigma_{\rm R}$. F_0 is a normalization constant $F_0 = \int D_{\rm eff}(B){\rm d}B$. Within the semi-classical perturbation theory, a semi-classical formula for the backward scattering ($\theta = \pi$) is given[12,40],

$$\begin{aligned}&\frac{{\rm d}\sigma_{\rm el}}{{\rm d}\sigma_{\rm R}}(E_{\rm c.m.}, B)\\ &= \left(1 + \frac{V_{\rm N}(R_{\rm c})}{E_{\rm c.m.}}\sqrt{\frac{Z_1Z_2e^2}{E_{\rm c.m.}}\frac{\pi}{a}}\right)\\ &\times \frac{\exp\left[-\frac{2\pi}{\hbar\omega}(E_{\rm c.m.} - B)\right]}{1 + \exp\left[-\frac{2\pi}{\hbar\omega}(E_{\rm c.m.} - B)\right]}, \end{aligned} \quad (35)$$

where the nuclear potential $V_{\rm N}(R_{\rm c})$ is evaluated at the Coulomb turning point,

$$\begin{aligned}V_{\rm N}(R_{\rm c}) = &\left(B - \frac{Z_1Z_2e^2}{R_{\rm f}}\right)\\ &\times\left(\frac{1 + \exp[(R_{\rm f} - R_0)/a]}{1 + \exp[(R_{\rm c} - R_0)/a]}\right), \end{aligned} \quad (36)$$

with the distance of the closest approach between two nuclei $R_{\rm c} = Z_1Z_2e^2/E_{\rm c.m.}$. a is the diffuseness parameter of the nuclear potential. Z_1, Z_2, $E_{\rm c.m.}$ denote the charge numbers of the projectile and target nuclei and the center-of-mass energy, respectively. R_f and $\hbar\omega$ are the barrier position and curvature of the modified Woods-Saxon potential, respectively.

The correction term $P_{\rm corr}$ in eq. (33) takes into account some effects in the quasi-elastic scattering that are not involved in the empirical barrier distribution (which was proposed for describing fusion reactions). In this work, we assume that the correction term mainly comes from nucleons transfer. In principle, the transfer process also affects the fusion process and the effect of nucleons transfer may have been implicitly taken into account in the empirical barrier distribution. However the influence of nucleons transfer on the quasi-elastic scattering may differ from the influence on the fusion process, and a small correction term seems to be required.

We assume the $P_{\rm corr}$ approximately equals the transfer probabilities $P_{\rm tr}$. The detailed introduction about the calculation of $P_{\rm tr}$ is in ref. [5]. Both the fusion and quasi-elastic scattering cross sections of a series of reactions have been studied with the proposed approach in this work. Figure 8 shows the calculated quasi-elastic scattering and fusion cross sections for the reactions ^{16}O+^{92}Zr, ^{16}O+^{186}W. The experimental data are also presented for comparison. The solid circles and squares denote the measured fusion cross sections $\sigma_{\rm fus}$ and large-angle quasi-elastic scattering cross sections, respectively. The solid curves in Figures 8(a) and (c) denote the calculated results for $\sigma_{\rm fus}$ with the proposed empirical barrier distribution (see details in refs. [1,4]). The crossed curves in Figures 8(b) and (d) denote the calculated quasi-elastic scattering cross sections with eq. (33). The dashed curves denote the results for $P_{\rm eff}$, i.e. the contribution of the empirical barrier distribution to the quasi-elastic scattering. We find that both the fusion excitation functions and the quasi-elastic scattering excitation functions of the four reactions can be satisfactorily well reproduced. More calculation results are given in ref. [5]. Figure 8 indicates that the modified Woods-Saxon potential together with the empirical barrier distribution can simultaneously describe the quasi-elastic scattering and fusion reactions reasonably well.

2.4 Influence of the shape of barrier distribution on fusion and quasi-elastic scattering

We further study the influence of the shape of the barrier distribution on the fusion cross section and the quasi-elastic scattering cross section. Here, the fusion and quasi-elastic scattering cross sections are calculated with

$$\begin{aligned}&\sigma_{\rm fus}(E_{\rm c.m.})\\ &= \frac{1}{F_0}\int_0^\infty D(B)\,\sigma_{\rm fus}^{\rm Wong}(E_{\rm c.m.}, B){\rm d}B, \end{aligned} \quad (37)$$

and

$$\begin{aligned}&\frac{{\rm d}\sigma_{\rm qel}}{{\rm d}\sigma_{\rm R}}(E_{\rm c.m.})\\ &= \frac{1}{F_0}\int_0^\infty D(B)\frac{{\rm d}\sigma_{\rm el}}{{\rm d}\sigma_{\rm R}}(E_{\rm c.m.}, B){\rm d}B + P_{\rm corr}, \end{aligned} \quad (38)$$

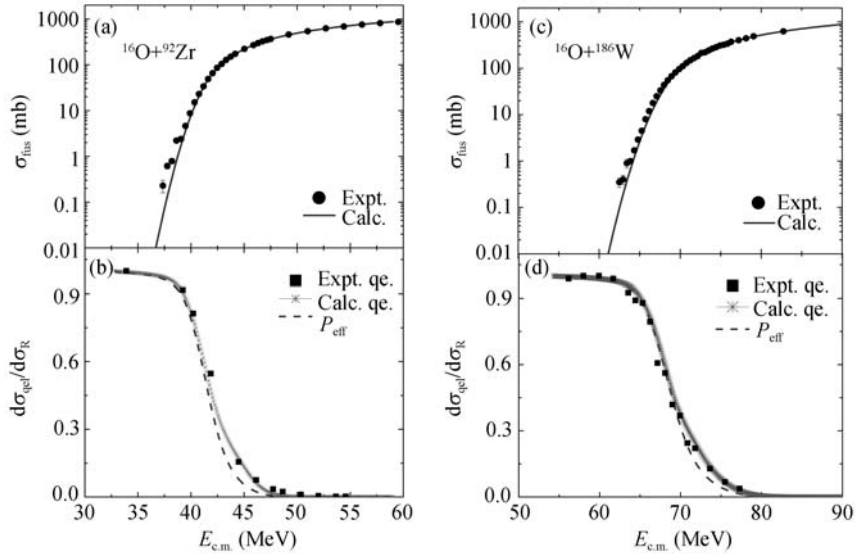

Figure 8 Fusion cross sections and quasi-elastic scattering cross sections as a function of energy for the reactions ^{16}O+^{92}Zr and ^{16}O+^{186}W. The solid circles and squares denote the measured fusion cross sections $\sigma_{\rm fus}$ and quasi-elastic scattering cross sections, respectively. The solid curves in (a) and (c) denote the calculated results for $\sigma_{\rm fus}$. The crossed curves in (b) and (d) denote the calculated results with eq. (33). The dashed curves denote the results for $P_{\rm eff}$. The experimental data are taken from refs. [14,15,41].

with $F_0 = \int D(B)\mathrm{d}B$. Figure 9 shows the comparison of the calculated fusion excitation function and the quasi-elastic scattering cross sections with $D(B) = D_1(B)$ (dash-dotted curves) and $D(B) = D_{\rm eff}(B)$ (solid curves) for the reaction ^{16}O+^{144}Sm. From the sub-figure of Figure 9(a), one can see that the left sides of the two barrier distributions D_1 and $D_{\rm eff}$ are close to each other while their right sides are quite different, the calculated fusion excitation functions shown in Figure 9(a) have not very large difference (the results with D_1 are a little higher than the experimental data at energies near and above the barrier). However, the calculated large-angle quasi-elastic scattering cross sections with the two barrier distributions D_1 and $D_{\rm eff}$ show very obvious difference. The results with D_1 can not reproduce the experimental data at energies around the barrier. To illustrate this point more clearly, we compare the calculation results of fusion and quasi-elastic scattering for the reaction ^{48}Ca+^{208}Pb with the barrier distribution obtained by different approaches. In the sub-figure of Figure 10(a), we show the barrier distributions of our approach (the solid curve) and of Zagrebeav[7] (the dash-dotted curve), respectively. We find that the capture cross sections obtained with two different barrier distributions are very close to each other, though there exists very large difference on the right sides of the barrier distributions. Both of them can reproduce the experimental data very well. However, the obtained large-angle quasi-elastic scattering cross sections are different at energies around the barrier which can be seen clearly in Figure 10(b). We suggest to measure the quasi-elastic scattering cross sections of ^{48}Ca+^{208}Pb to test these two barrier distributions.

Figures 9 and 10 indicate that the fusion cross sections depend more strongly on the shape of the left side of the barrier distribution while the quasi-elastic scattering cross sections depend more strongly on that of the right side. This conclusion has already been given by the difference of the statistic errors of the extracted barrier distributions from the fusion excitation functions and from the quasi-elastic scattering cross sections, respectively. The former increases with incident energies while the latter decreases with energies[16]. The calculations demonstrate that the non-symmetric empirical barrier distribution is reasonable and necessary for a unified description of fusion and

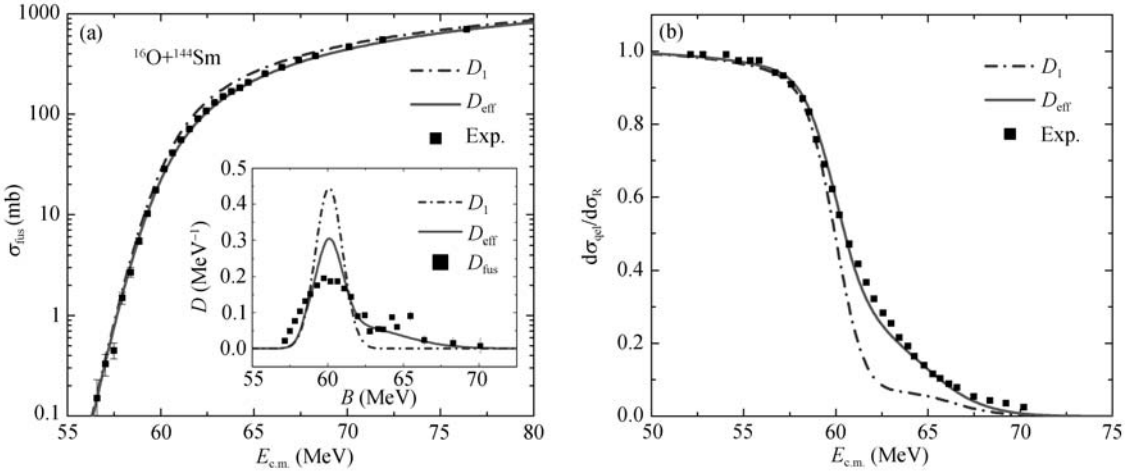

Figure 9 Comparison of the calculated fusion excitation function and the quasi-elastic scattering cross sections with $D(B) = D_1(B)$ (dash-dotted curves) and $D(B) = D_{\rm eff}(B)$ (solid curves) for the reaction ^{16}O+^{144}Sm. The experimental data of fusion and quasi-elastic scattering are taken from refs. [14,15], respectively.

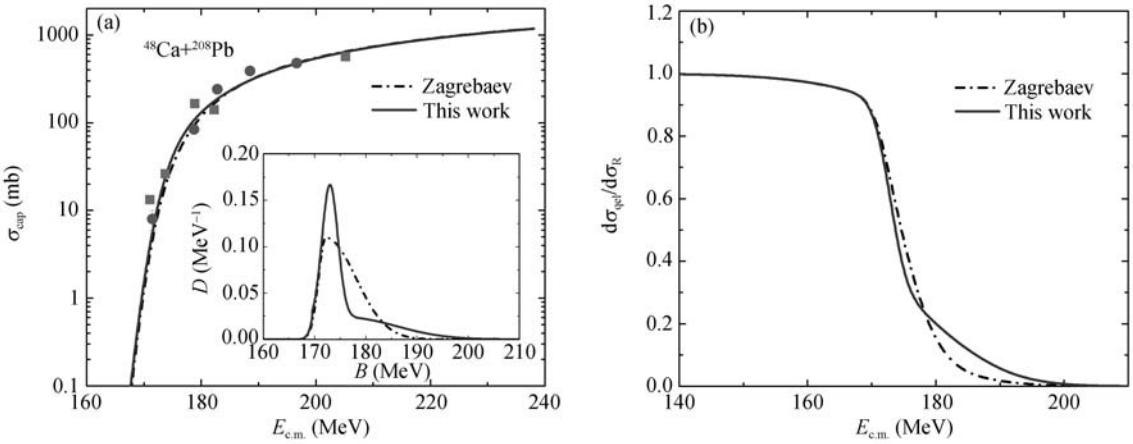

Figure 10 Comparison of the calculated fusion excitation function and the quasi-elastic scattering cross sections with the barrier distribution proposed in this work (solid curves) and Zagrebeav's barrier distribution[7] (dash-dotted curves) for the reaction ^{48}Ca+^{208}Pb. The experimental data (squares and full circles) are taken from refs. [42,43].

quasi-elastic scattering.

3 Application of the model to fusion-fission reactions

In this section, we apply the Skyrme energy density functional approach to study the fusion-fission reactions (region II in Figure 1). Firstly, the statistical model HIVAP is briefly introduced and the influence of some key parameters is studied. Then, a number of calculated results are compared with experimental data, Finally, the formation probability of compound nucleus is deduced based on the measured evaporation residue cross sections for "cold" and "hot" fusion.

3.1 Fission barrier and level density parameters in evaporation calculations

The calculations of the survival probabilities $W_{\rm sur}$ of the compound nuclei were performed with the statistical evaporation code called HIVAP which uses standard evaporation theory and takes into account the competition of γ-ray, neutron, proton, α-particle emission with fission using angular-

momentum and shape-dependent two-Fermi-gas-model level density formula[21]. Although it is a standard statistical model for describing the de-excitation process, one has to reconsider some parameters adopted for describing a wide range of fusion-fission reactions. The sensitive parameters involved are primarily fission barriers and level density parameters.

In the standard HIVAP code, the fission barrier at zero angular momentum is calculated by

$$B_{\rm f} = B_{\rm f}^{\rm mac} - S. \tag{39}$$

The macroscopic barrier $B_{\rm f}^{\rm mac}$ is usually described with a liquid-drop model refined by Cohen and Swiatecki[44], Sierk[45], and Dahlinger et al.[46]. The shell correction S is calculated from the difference of the experimental mass and the liquid-drop mass, $S = M_{\rm exp} - M_{\rm LD}$. In this code, the liquid-drop mass is calculated with the parameter set proposed by Myers and Swiatecki in 1967, and the $M_{\rm exp}$ is in fact taken from the mass table of Möller-Nix[48] which was obtained with the finite range droplet model and has an rms deviation of only 0.656 MeV for 2149 measured masses of nuclei[49].

In the present work, we calculate the macroscopic fission barriers with the proposed modified Woods-Saxon (MWS) potential model in which the parameters of MWS potential are obtained based on the Skyrme energy density functional. The value of $B_{\rm f}^{\rm mac}$ is empirically estimated by the depth of the potential pocket, as shown as an example in Figure 11. This figure is for the $^{256}_{102}$No (formed in reaction ^{48}Ca+^{208}Pb) fissioning into two $^{128}_{51}$Sb. The obtained barrier is 1.74 MeV. The corresponding data from refs. [44–46] are 1.44, 1.02 and 1.19 MeV, respectively. The barrier for ^{244}Pu from our method and from refs. [44–46] are 4.16, 5.17, 3.95 and 4.13 MeV, respectively. The deviations between our calculated results and the results of liquid-drop models for heavy nuclei are in a permitting region. To see it more clearly, in Figure 12 we show the comparison of the macroscopic fission barriers obtained with different models for a series of nuclei along the β-stability line which is approximately determined by the formula $Z = A/2[1 - 0.4A/(A + 200)]$. For heavy nuclei the four models give similar trend. The results of MWS potential are slightly higher in the region $260 < A < 294$, and sharply decrease when $A > 300$. For medium mass nuclei, our results are in agreement with those of refs. [50,51] in which the reduction of the liquid-drop barriers was discussed.

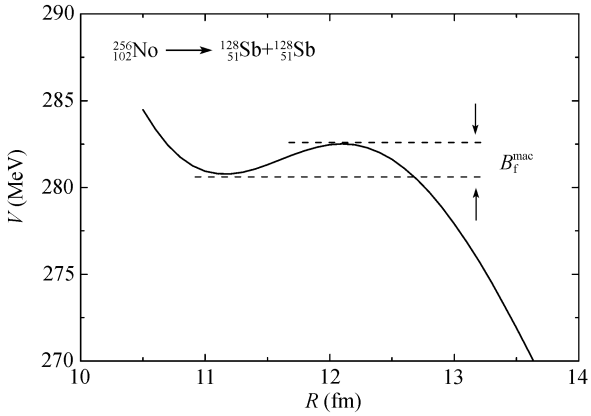

Figure 11 The macroscopic fission barrier $B_{\rm f}^{\rm mac}$ for $^{256}_{102}$No fissioning into two $^{128}_{51}$Sb obtained with the modified Woods-Saxon potential.

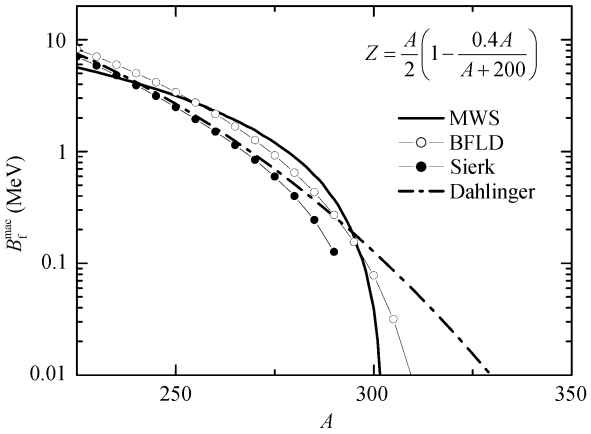

Figure 12 The macroscopic fission barrier $B_{\rm f}^{\rm mac}$ for nuclei along the β-stability line obtained with different models. The solid curve, the open circles, the solid circles and the dash-dotted curve denote the results of the modified Woods-Saxon potential, Cohen and Swiatecki[44], Sierk[45], and Dahlinger et al.[46], respectively.

We know that the nuclear shapes during fission are more elongated than during fusion. In this empirical approach, the neck and elongation of the system at fission configuration can not be described well in the sudden approximation. We concentrate on the height of the fission barrier in this method. We will systematically investigate

51 fusion-fission reactions with the fission barriers obtained with four different models (MWS potential model, Cohen-Swiatecki's[44], Sierk's[45] and Dahlinger's[46] methods). The results will be discussed in the following paragraph.

In this code, the level density is[20]

$$\rho(J,E^*) = \frac{1}{24}\left(\frac{\hbar^2}{2\theta}\right)^{3/2}(2J+1)a^{1/2}U_J^{-2} \times \exp[2(aU_J)^{1/2}], \quad (40)$$

$$U_J = E^* - E_r(J). \quad (41)$$

Here $E_r(J)$ is the yrast energy of either the equilibrium configuration (light-particle and γ-emission) or the saddle-point configuration (fission) and reads

$$E_{\rm r}(J) = J(J+1)\hbar^2/2I, \quad (42)$$

in which I is the moment of inertia. The level density parameter a is obtained from[11] as

$$a = \tilde{a}[1 + f(E^*)S/E^*], \quad (43)$$

with

$$f(E^*) = 1 - \exp(-E^*/E_{\rm d}) \quad (44)$$

with the shell damping energy $E_{\rm d}$ being 18.5 MeV[20]. In the standard HIVAP code, the *smooth*, shell-independent level-density parameter reads

$$\tilde{a} = 0.04543\ r_{\rm a}^3 A + 0.1355\ r_{\rm a}^2 A^{2/3} B_S + 0.1426\ r_{\rm a} A^{1/3} B_K, \quad (45)$$

which takes into account the volume, surface and curvature dependence of the single-particle level density at the Fermi surface. B_S and B_K denote the surface and curvature factors defined in the droplet model[47]. For evaporation channels we set $B_S = B_K = 1$. For the fission channel, the values of B_S and B_K are tabulated as a function of the fissility parameter in ref. [47]. The ratio $\tilde{a}_{\rm f}/\tilde{a}_{\rm n}$ ($\tilde{a}_{\rm f}$ level density parameter for fission channel, $\tilde{a}_{\rm n}$ for neutron channel) is larger than 1. It decreases towards a unit with the increase of the fissility parameter. The results of $\tilde{a}_{\rm f}/\tilde{a}_{\rm n}$ for a series of nuclei in ref. [20] can be well reproduced. $r_{\rm a}$ is the radius parameter found to be $r_{\rm a} = 1.153$ fm[20].

With this parametrization 51 fusion-fission reactions have been systematically investigated with the MWS, Cohen-Swiatecki's, Sierk's and Dahlinger's fission barriers, respectively, incorporating the proposed approach for describing the fusion (capture) cross sections (see eq. (24)). Calculations of the fission and particle emission widths with the traditional statistical theory were introduced in ref. [50]. The average deviation $\chi^2_{\log}$ (see eq. (28)) of the evaporation (and fission) cross sections from the experimental data for these reactions are listed in Table 2. We find that the average deviation obtained with the MWS potential is much smaller than those obtained with the other barriers. By varying the volume, surface and curvature coefficients in eq. (45) and the damping energy $E_{\rm d}$, and searching for the minimum of $\chi^2_{\log}$ with the MWS fission barriers, we find that the values proposed by Reisdorf[20] (adopted in the present work) are very close to the corresponding optimal ones. In some references the shell damping energy was written as $E_{\rm d} = k_0 A^{1/3}$ or similar forms. We find that the minimal deviation is not much improved by changing the value of the coefficient k_0. Therefore, in our calculations we consequently keep Reisdorf's coefficients, eq. (45), that contains only one empirically adjustable parameter $r_{\rm a}$.

Table 2 Average deviation of the evaporation (and fission) cross sections from experimental data for 51 fusion-fission reactions with $r_{\rm a} = 1.153$ fm

Model	Cohen-Swiatecki	Sierk	Dahlinger	MWS
$\chi^2_{\log}$	0.2295	0.2177	0.2373	0.1339

Through a variation of r_a we can find the optimal values of r_a for a certain model to describe the fission barriers. The optimal value of r_a could be different for different fission barrier models. Through systematical investigation of the minimal average $\chi^2_{\log}$ of the 51 fusion-fission reactions, we search for the optimal parameters set (including the parameters of fission barrier and the r_a in level density parameter). The minimal average $\chi^2_{\log}$ of the 51 reactions and the corresponding optimal values of $r_{\rm a}$ for the four fission barrier models are listed in Table 3. By taking the optimal values of $r_{\rm a}$, the average deviations $\chi^2_{\log}$ from the experimental data get obviously smaller for all of these models, especially for the models of Sierk and Dahlinger. The

deviation obtained by the modified Woods-Saxon potential is still the smallest one.

Table 3 The minimal average deviation $\chi^2_{\log}$ and the corresponding optimal value of r_a adopting different models for calculating the fission barriers

Model	Cohen-Swiatecki	Sierk	Dahlinger	MWS
$\chi^2_{\log}$	0.1813	0.1428	0.1642	0.1086
r_a	1.106	1.091	1.095	1.120

Finally, we obtain the optimal parameters set of the HIVAP code: MWS potential model for the fission barriers, with $r_a = 1.120$ fm and together with the 1967 parametrization of the liquid-drop energies of nuclei for the shell corrections.

3.2 Comparison between the calculated results and the experimental data

With the modified Woods-Saxon potential for the unified description of the entrance channel fusion barrier and the macroscopic fission barrier B_f^{MWS}, with $r_a = 1.120$ fm, and together with the 1967 parametrization of Mayers and Swiatecki for the shell corrections, we obtain the deviations $\chi^2_{\log}$ of the evaporation (and fission) cross sections from the experimental data for the 51 fusion-fission reactions which are shown in Figure 13. We find that 68.3% reactions have values smaller than 0.0714, with which we can estimate the upper and lower confidence limits of the systematic errors of the HIVAP code for W_{sur} (the values are $1.85W_{sur}$ and $W_{sur}/1.85$, respectively). In Figure 14, we present the calculated results together with the systematic errors (the shades in the figures) of σ_{fus} and W_{sur}[4]. The experimental data are also presented for comparison. One finds that the experimental data can be systematically well reproduced (within about 2 times deviations) at energies near and above the fusion barriers.

Figure 15 shows calculated neutron evaporation residue cross sections for heavy systems with ^{208}Pb[4]. Because the quasi-fission has not been taken into account in these calculations yet, we find that the deviations from the experimental data increase exponentially with the increase of Z_{CN} (the positions of the peaks for the evaporation residues can be roughly reproduced). This implies that the quasi-fission plays an important role in the reactions leading to superheavy nuclei. With the proposed approach for σ_{cap} and W_{sur}, the ambiguity in predicting the probability of quasi-fission (or the formation probability P_{CN} of compound nucleus) could be reduced.

With the proposed approach for calculating the capture cross sections σ_{cap} and the survival probabilities W_{sur} of the compound nuclei, one may deduce the value of the formation probabilities P_{CN} of the compound nuclei from the measured evaporation residue cross sections σ_{ER} of some superheavy nuclei produced in "cold" fusion or "hot" fusion according to eq. (1). Because the dependence of P_{CN} on the incident energy of the reaction system is not so clear and the available experimental data are very limited in present, it is difficult (even impossible) to obtain the exact values of P_{CN} presently. Here, we just give some very preliminary and rough estimation of the mean values of P_{CN} in the region $B_{m.p.} < E_{c.m.} < B_0$[52]. Here, $B_{m.p.}$ denotes the most probable barrier height based on the barrier distribution $D_{eff}(B)$. B_0 is the barrier height of the entrance channel potential. Figure 16 shows the deduced mean values of logarithm of P_{CN} (which gives the order of magnitude of P_{CN}) as a function the charge number of the compound nucleus. The squares denote the results with the "cold" fusion, i.e., the reactions with Pb and Bi targets[54−56]. The open circles denote the results with the "hot" fusion, i.e., the reactions with ^{48}Ca bombarding on actinite targets[57,58]. The error bars are roughly estimated by the systematic errors in the σ_{cap}

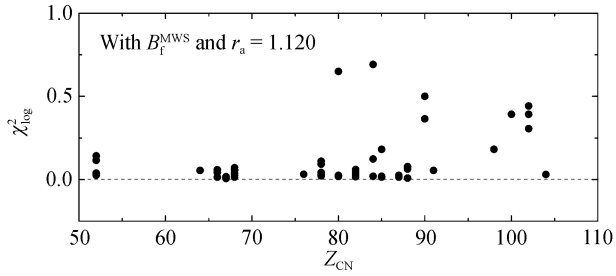

Figure 13 Deviations $\chi^2_{\log}$ of the calculated evaporation (and fission) cross sections from the experimental data for 51 fusion-fission reactions.

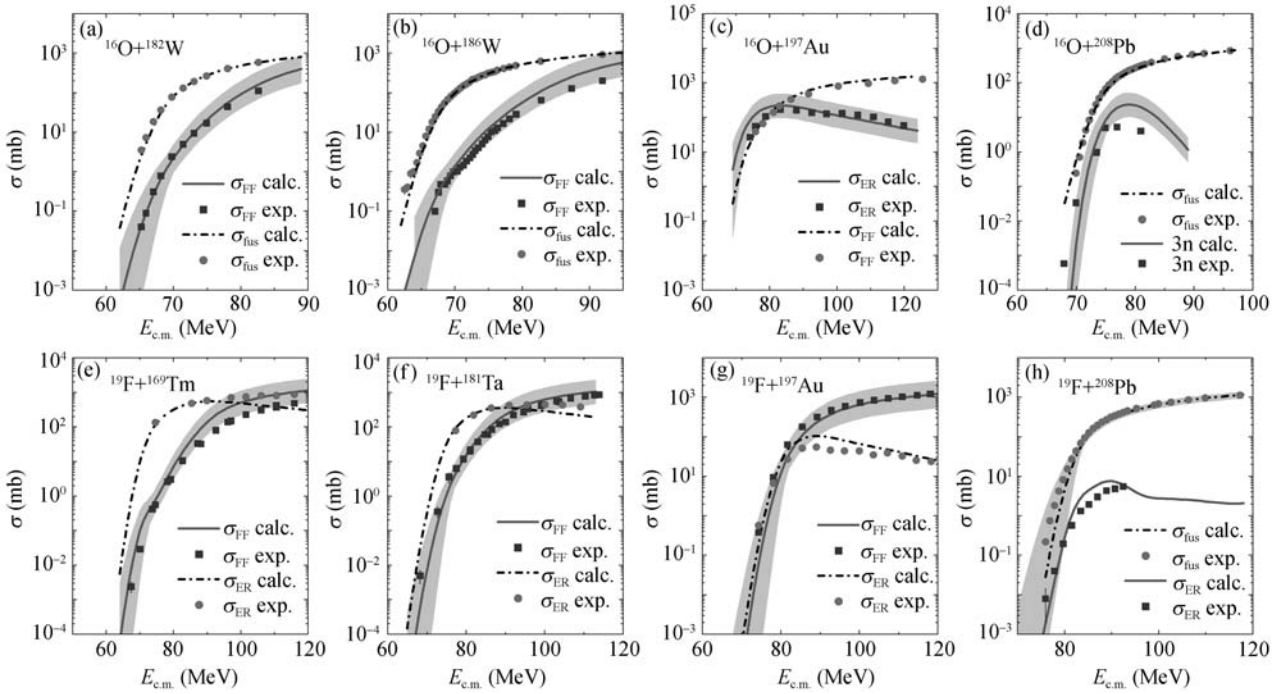

Figure 14 The cross sections of reactions ^{16}O+^{182,186}W, ^{16}O+^{197}Au, ^{16}O+^{208}Pb, ^{19}F+^{169}Tm, ^{19}F+^{181}Ta, ^{19}F+^{197}Au and ^{19}F+^{208}Pb. The shade in (h) denotes the systematic errors of the capture cross sections. σ_{FF} denotes the fission cross section. σ_{ER} denotes the evaporation residue cross section (a sum over all evaporation channels). The shades in (a)–(g) denote the systematic errors of the present approach (including both the systematic errors of σ_{cap} and those of W_{sur}).

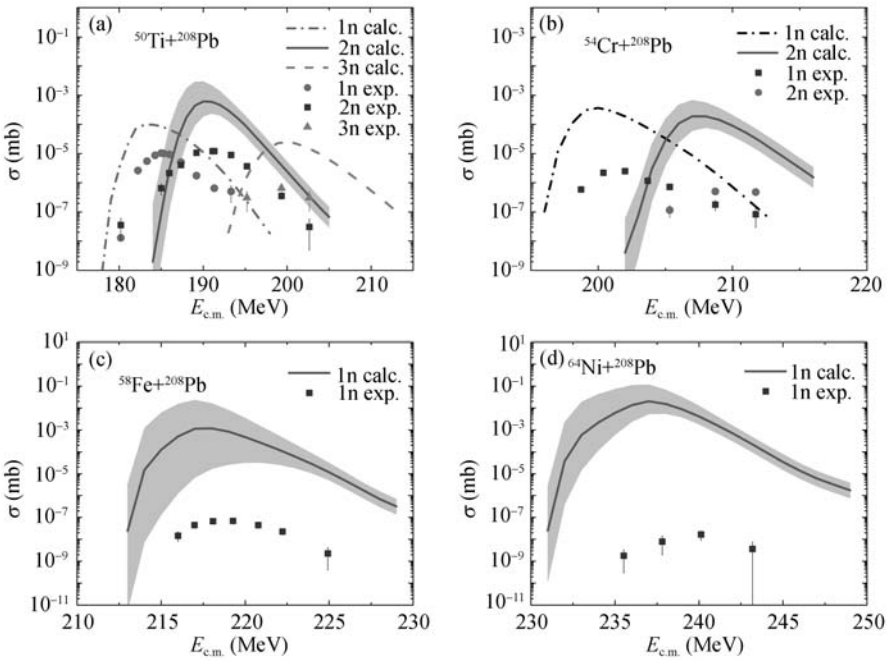

Figure 15 The neutron evaporation residue cross sections of heavy reactions with ^{208}Pb target. The quasi-fission is not taken into account in the calculation.

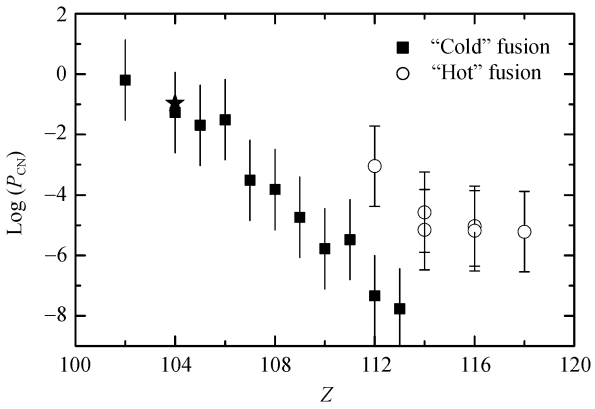

Figure 16 The deduced mean value of the logarithm of $P_{\rm CN}$ as a function of the compound-nuclear charge number. The squares and open circles denote the results with "cold" fusion and "hot" fusion, respectively. The star denotes the corresponding result of the deduced mean value of the logarithm of $P_{\rm CN}$ around the Coulomb barrier in ref. [54]. The experimental data of evaporation cross sections are taken from refs. [55–58].

and $W_{\rm sur}$, and the error bars of the measured $\sigma_{\rm ER}$. One can see that the $P_{\rm CN}$ exponentially decreases with the charge number generally in the "cold" fusion reactions. However, the decrease of the $P_{\rm CN}$ with Z is not very obvious in the region $Z \geqslant 114$ in the "hot" fusion reactions. The star denotes the result of the deduced mean value of logarithm of $P_{\rm CN}$ around the Coulomb barrier for ^{50}Ti+^{208}Pb in ref. [53]. It is encouraging to note that the two methods of deducing $P_{\rm CN}$ give similar results for this system.

4 Conclusion and discussion

In this work, we give a brief review of the Skyrme energy density functional approach which has been applied to study heavy-ion fusion and scattering reactions. The properties of ground state nuclei are studied with the Skyrme energy density functional together with the semi-classical extended Thomas-Fermi approach (up to the second order in $\hbar$). With the proton and neutron density distributions obtained in this way, the fusion barriers of a series of reaction systems are calculated by the same Skyrme energy density functional. We propose an empirical barrier distribution which is based on the fusion barrier calculated with the Skyrme energy density functional and is assumed to be the superposition of two Gaussian functions. With the empirical barrier distribution, a large number fusion, fusion-fission and quasi-elastic scattering reactions have been studied systematically. 1) A large number of measured fusion excitation functions for light and medium-heavy fusion systems around the fusion barriers can be reproduced well. In the calculated the fusion (capture) excitation functions of 120 fusion reactions at energies near and above the barrier, about 70% systems have very small deviations from the experimental data. 2) All of calculations adopt the same parameters (Skyrme force SkM* and several parameters in the empirical barrier distribution) without any adjustable parameters. 3) The shell effects and neutron-rich effects which influence the fusion cross sections at sub-barrier energies have been taken into account by the structure effect factor g empirically. 4) An analytical expression with Woods-Saxon form for the nucleus-nucleus potential is proposed based on the entrance channel fusion potential obtained by the Skyrme energy density functional approach. 5) The elastic scattering angle distributions of a series of reactions at energies much higher than the Coulomb barrier can be reasonably well reproduced by the modified Woods-Saxon potential which is based on the frozen density approximation systematically. 6) With the same empirical barrier distribution and taking into account the correction term that mainly comes from the nucleons transfer, the calculated large-angle quasi-elastic scattering cross sections of these reactions are in good agreement with the experimental data. 7) The fusion cross sections depend more strongly on the shape of the left side of the barrier distribution while the quasi-elastic scattering cross sections depend more strongly on the right side. 8) Incorporating a statistical model HIVAP for describing the decay of the compound nuclei, the evaporation residue (and fission) cross sections of 51 fusion-fission reactions have been systematically studied simultaneously to investigate and refine some key parameters of the HIVAP code. The experimental data can be systematically re-

produced reasonably well. 9) The mean value of the fusion probability $P_{\rm CN}$ is roughly deduced from the measured evaporation residue cross sections. The obtained $P_{\rm CN}$ decreases exponentially with the charge number of the compound nucleus generally in "cold" fusion while the decrease is not very obvious in the region $Z \geqslant 114$ in "hot" fusion.

The authors would like to give special thanks to Prof. En-Guang Zhao for helpful discussions and encouragements. We also thank Prof. Shan-Gui Zhou for valuable suggestions and a careful reading of the manuscript.

1 Liu M, Wang N, Li Z, et al. Applications of Skyrme energy-density functional to fusion reactions spanning the fusion barriers. Nucl Phys A, 2006, 768: 80–98

2 Wang N, Wu X, Li Z, et al. Applications of Skyrme energy-density functional to fusion reactions for synthesis of superheavy nuclei. Phys Rev C, 2006, 74: 044604

3 Wang N, Li Z, Scheid W. Systematic study of fusion barriers. J Phys G-Nucl Part Phys, 2007, 34: 1935–1953

4 Wang N, Zhao K, Scheid W, et al. Phys Rev C, 2008, 77: 014603, and references therein

5 Wang N, Scheid W. Quasi-elastic scattering and fusion with a modified Woods-Saxon potential. Phys Rev C, 2008, 78: 014607

6 Shen C, Kosenko G, Abe Y. Two-step model of fusion for the synthesis of superheavy elements. Phys Rev C, 2002, 66: 061602

7 Zagrebaev V I. Synthesis of superheavy nuclei: Nucleon collectivization as a mechanism for compound nucleus formation. Phys Rev C, 2001, 64: 034606

8 Adamian G G, Antonenko N V, Scheid W, et al. Fusion cross sections for superheavy nuclei in the dinuclear system concept. Nucl Phys A, 1998, 633: 409–420

9 Feng Z, Jin G, Fu F, et al. Production cross sections of superheavy nuclei based on dinuclear system model. Nucl Phys A, 2006, 771: 50–67

10 Siwek-Wilczynska K, Skwira I, Wilczyński J. Tests of the fission-evaporation competition in the deexcitation of heavy nuclei. Phys Rev C, 2005, 72: 034605

11 Reisdorf W, Hessberger F P, Hildenbrand K D, et al. Fusability and fissionability in 86Kr-induced reactions near and below the fusion barrier. Nucl Phys A, 1985, 444: 154–188

12 Hagino K, Rowley N. Large-angle scattering and quasielastic barrier distributions. Phys Rev C, 2004, 69: 054610

13 Rowley N, Satchler G R, Stelson P H. On the "distribution of barriers" interpretation of heavy-ion fusion. Phys Lett B, 1991, 254: 25–29

14 Leigh J R, Dasgupta M, Hinde D J, et al. Barrier distributions from the fusion of oxygen ions with 144,148,154Sm and 186W. Phys Rev C, 1995, 52: 3151–3166

15 Timmers H, Leigh J R, Dasgupta M, et al. Probing fusion barrier distributions with quasi-elastic scattering. Nucl Phys A, 1995, 584: 190-204

16 Timmers H, Leigh J R, Rowley N, et al. Barrier distributions and scattering. J Phys G-Nucl Part Phys, 1997, 23: 1175–1181

17 Bartel J, Brack M, Durand M. Extended Thomas-Fermi theory at finite temperature. Nucl Phys A, 1985, 445: 263–303

18 Brack M, Guet C, Hakanson H B. Selfconsistent semiclassical description of average nuclear properties: A link between microscopic and macroscopic models. Phys Rep, 1985, 123: 275–364

19 Bartel J, Bencheikh K. Nuclear mean fields through self-consistent semiclassical calculations. Eur Phys J, 2002, A14: 179–190

20 Reisdorf W. Analysis of fissionability data at high excitation energies. Z Phys A, 1981, 300: 227–238

21 Reisdorf W, Schädel M. How well do we understand the synthesis of heavy elements by heavy-ion induced fusion? Z Phys A, 1992, 343: 47–57

22 Vautherin D, Brink D M. Hartree-Fock calculations with Skyrme's interaction. I. Spherical Nuclei. Phys Rev C, 1972, 5: 626–647

23 Denisov V Y, Noerenberg W. Entrance channel potentials in the synthesis of the heaviest nuclei. Eur Phys J A, 2002, 15: 375–388

24 Bartel J, Quentin P, Brack M, et al. Towards a better parametrisation of Skyrme-like effective forces. Nucl Phys A, 1982, 386: 79–100

25 Liu M, Wang N, Li Z, et al. Neutron skin thickness of nuclei and effective nucleon-nucleon interactions. Chin Phys Lett, 2006, 23: 804–807

26 Myers W D, Swiatecki W J. Nucleus-nucleus proximity potential and superheavy nuclei. Phys Rev C, 2000, 62: 044610

27 Stelson P H. Neutron flow between nuclei as the principal enhancement mechanism in heavy-ion subbarrier fusion. Phys Lett B, 1988, 205: 190–194

28 Timmers H, Ackermann D, Beghini S, et al. A case study of collectivity, transfer and fusion enhancement. Nucl Phys A, 1998, 633: 421–445

29 Wang N, Li Z, Wu X. Improved quantum molecular dynamics model and its applications to fusion reaction near barrier. Phys Rev C, 2002, 65: 064608

30 Wong C Y. Interaction barrier in charged-particle nuclear reactions. Phys Rev Lett, 1973, 31: 766–769

31 Washiyama K, Lacroix D. Energy dependence of the nucleus-nucleus potential close to the Coulomb barrier. Phys Rev C, 2008, 78: 024610

32 Yang Y, Li Q. ^{16}O+^{16}O elastic scattering in an α-folding model. Phys Rev C, 2005, 72: 054603

33 Santra S, Singh P, Kailas S, et al. Coupled reaction channel analysis of elastic, inelastic, transfer, and fusion cross sections for ^{12}C+^{208}Pb. Phys Rev C, 2001, 64: 024602

34 Sahm C C, Murakami T, Cramer J G, et al. Total reaction

cross section for ^{12}C on ^{12}C, ^{40}Ca, ^{90}Zr, and ^{208}Pb between 10 and 35 MeV/nucleon. Phys Rev C, 1986, 34: 2165–2170
35 Videbaek F, Goldstein R B, Grodzins L, et al. Elastic scattering, transfer reactions, and fission induced by ^{16}O ions on ^{181}Ta and ^{208}Pb. Phys Rev C, 1977, 15: 954–971
36 Ball J B, Fulmer C B, Gross E E, et al. Heavy ion elastic scattering survey: (I). ^{208}Pb target. Nucl Phys A, 1975, 252: 208–236
37 Lichtenthäler R, Pereira D, Chamon L C, et al. Second order effects in the algebraic potential for heavy-ion systems near the Coulomb barrier. Phys Rev C, 1994, 50: 3033–3036
38 Andres M V, Rowley N, Nagarajan M A. Effect of deformation on the elastic and quasielastic scattering of heavy ions near the Coulomb barrier. Phys Lett B, 1988, 202: 292–295
39 Zhang H, Yang F, Lin C, et al. Barrier distributions for ^{16}O+^{152}Sm quasielastic and elastic scattering. Phys Rev C, 1998, 57: R1047–R1050
40 Landowne S, Wolter H H. On sub-Coulomb heavy-ion scattering and the problem of nuclear absorption. Nucl Phys A, 1981, 351: 171–188
41 Newton J O, Morton C R, Dasgupta M, et al. Experimental barrier distributions for the fusion of ^{12}C, ^{16}O, ^{28}Si, and ^{35}Cl with ^{92}Zr and coupled-channels analyses. Phys Rev C, 2001, 64: 064608
42 Prokhorova E V, Cherepanov E A, Itkis M G, et al. arXiv:nucl-ex/0309021
43 Pacheco A J, Fernández Niello J O, DiGregorio D E, et al. Capture reactions in the ^{40,48}Ca+^{197}Au and ^{40,48}Ca+^{208}Pb systems. Phys Rev C, 1992, 45: 2861–2869
44 Cohen S, Swiatecki W J. The deformation energy of a charged drop: Part V: Results of electronic computer studies. Ann Phys (N.Y.), 1963, 22: 406–437
45 Sierk A. Macroscopic model of rotating nuclei. Phys Rev C, 1986, 33: 2039–2053
46 Dahlinger M, Vermeulen D, Schmidt K H. Empirical saddle-point and ground-state masses as a probe of the droplet model. Nucl Phys A, 1982, 376: 94–130
47 Myers W D, Swiatecki W J. The nuclear droplet model for arbitrary shapes. Ann Phys, 1974, 84: 186–210
48 Möller P, Nix J R, Myers W D, et al. Nuclear ground-state masses and deformations. At Data Nucl Data Tables, 1995, 59: 185–381
49 Buchinger F, Pearson J M. Charge radii in macroscopic-microscopic mass models. Phys Rev C, 2005, 72: 057305
50 Beckerman M, Blann M. Fission barrier in charged-particle nuclear reactions. Phys Rev Lett, 1977, 38: 272–275
51 Beckerman M, Blann M. Statistical-model analyses of heavy-ion-induced fusion reaction products. Phys Rev C, 1978, 17: 1615–1631
52 Tian J, Wang N, Li Z. Modified Woods-Saxon potential for heavy-ion fusion reaction. Chin Phys Lett, 2007, 24: 905–908
53 Naik R S, Loveland W, Sprunger P H, et al. Measurement of the fusion probability PCN for the reaction of ^{50}Ti with ^{208}Pb. Phys Rev C, 2007, 76: 054604
54 Hofmann S, Ninov V, Hessberger F P, et al. Production and decay of ^{269}110. Hofmann S, Ninov V, Hessberger F P, et al. Production and decay of ^{269}110. Z Phys A, 1995, 350: 277–280; Z Phys A, 1995, 350: 281–282
55 Hofmann S, M nzenberg G. The discovery of the heaviest elements. Rev Mod Phys, 2000, 72: 733–767
56 Morita K. Superheavy research in Japan. Prog Part Nucl Phys, 2009, 62: 325–336
57 Oganessian Y T, Utyonkov V K, Lobanov Y V, et al. Synthesis of superheavy nuclei in the ^{48}Ca+^{244}Pu reaction: ^{288}114. Phys Rev C, 2000, 62: 041604(R); Oganessian Y T, Utyonkov V K, Lobanov Y V, et al. Observation of the decay of ^{292}116. Phys Rev C, 2000, 63: 011301(R)
58 Oganessian Y T, Utyonkov V K, Lobanov Y V, et al. Synthesis of the isotopes of elements 118 and 116 in the ^{249}Cf and ^{245}Cm+^{48}Ca fusion reactions. Phys Rev C, 2006, 74: 044602